Journal of Physics and Chemistry of Solids 155 (2021) 110125

Contents lists available at ScienceDirect

Journal of Physics and Chemistry of Solids

journal homepage: http://www.elsevier.com/locate/jpcs

# Efficient photocatalytic degradation of Malachite green dye using facilely synthesized cobalt oxide nanomaterials using citric acid and oleic acid

Monu Verma [a], Meena Mitan [b], Hyunook Kim [a], Dipti Vaya [c,*]

[a] Water-Energy Nexus Laboratory, Department of Environmental Engineering, University of Seoul, Seoul, 02504, Republic of Korea
[b] Department of Applied Sciences, The NorthCap University, Haryana, 122017, India
[c] Department of Chemistry, Amity School of Applied Science, Amity University, Haryana, 122413, India

ARTICLE INFO

*Keywords:*
Photocatalysis
Nanomaterials
Dye
Kinetics
Degradation

ABSTRACT

Citric acid and oleic acid modified cobalt oxide nanomaterials successfully fabricated by sol-gel process and used to remove malachite green (MG) by photocatalytic degradation. The synthesized nanomaterials were characterized by powder X-ray diffraction (P-XRD), Scanning electronic microscopy (SEM), Transmission electron microscopy (TEM), UV–Visible spectrophotometer, Fourier transform infrared spectroscopy (FT-IR) and Thermogravimetric Analysis (TGA) in order to investigate their structural, morphological, optical, functional and thermal properties, respectively. The PXRD gave the crystalline nature with average crystallite size of 29 and 42 nm for citric acid and oleic acid modified cobalt oxide nanomaterials, respectively. SEM images indicate layered porous aggregates morphology having higher porosity. Optimum condition for photocatalytic degradation of MG dye were found at pH 6.84, dose 0.5 $gL^{-1}$ for $1 \times 10^{-5}$ M concentrated dye. Citric acid modified cobalt oxide catalyst exhibited 91.2% photocatalytic degradation of MG dye while in oleic acid modified sample exhibited 66.6% under simulated light due to greater chelating power of citric acid as compare to oleic acid. Kinetics results for MG dye degradation follow to pseudo-second-order kinetics with rate constants 0.00653, 0.084 and 0.00633 $mol^{-1}L^{1}min^{-1}$ for CoCA, CoOA and Co NPs, respectively. In addition, possible mechanism for the photodegradation of MG dye is also proposed.

## 1. Introduction

Recently, due to rapid development of industries and social economy, non-biodegradable pollutants in aqueous system becomes more and more serious and greatly influenced the health people and animals [1]. Also, toxicity of pollutants could be assessed by using bacterial and plant bioassay such as Vibrio fischeri and Vicia faba respectively [2–4]. Dyes are also included in this category which are released from industrial sectors such as printing, food, textile, leather, paper, cosmetics, rubber, and pharmaceutical, and become a serious threat to the human health and environmental safety. These are carcinogenic in nature and are responsible for potential health hazards to living being. Among the different dyes, MG a synthetic cationic dye for both laboratory research as well as industrial products, and show higher toxicity [5]. Since MG capable to enter into cells due to its easy interaction with membranes [6]. It is widely used as an additive in food colouring and dye in varieties of industries [7,8]. Therefore, it is highly recommended to degrade the dyes into nontoxic forms. Different chemical, biological and physical processes have been used for the treatment of wastewater to get rid from dyes and related toxic pollutants. Some of the physico-chemical water treatment methods like flocculation, precipitation, membrane filtration, coagulation, ion-exchange and adsorption techniques are extensively used for removal pollutants, however, these are not ideal to remove he pollutants completely [9–13]. Heterogeneous photocatalysis is carried out using semiconductor oxides for complete mineralization of organic pollutants to $CO_2$, $H_2O$ and inorganic ions [14]. Photocatalysis gets good position as compared to other conventional methods in water treatment due to solar energy [15].

The nanomaterials possess unique physical and chemical properties such as higher surface area, surface defects etc. And, would be utilized in the photocatalytic process. Nanomaterials exhibit unique optical properties which usually dependent upon size and shape [16,17]. Cobalt oxides are utilized in various form such as lithium ion batteries, heterogeneous catalysts, gas sensor, ceramics, energy storage devices etc. [18–20].

Efficiency of heterogeneous catalyst increases by altering size,

* Corresponding author.
*E-mail address:* diptivaya08@gmail.com (D. Vaya).

https://doi.org/10.1016/j.jpcs.2021.110125
Received 2 February 2021; Received in revised form 28 March 2021; Accepted 18 April 2021
Available online 23 April 2021

distribution and morphology of nanoparticles. For the synthesis of Cobalt oxide nanoparticles (Co NPs) numerous methodologies are mentioned i.e. co-precipitation, sol-gel combined with thermal decomposition [21], hydrothermal [22], green synthesis [23,24], pulsed laser deposition [25] and solution combustion [26]. The sol-gel method has reported profusely as it offers modulated size, shape, distribution of nanoparticles and low temperature condition [27].

Small nanomaterials have an extremely high surface area to volume ratio and tendency to agglomerate. Hence, agglomeration can be prevented by capping [16,28]. Along with nature of capping agent, its critical concentration also deciding factor for the morphology of the synthesized particles [29]. Therefore, sol-gel along with capping agent is considered as simple, efficient and cost effective soft chemical route with monodisperse stable nanoparticles at low temperatures.

In the present work, two different types of capping agents: citric acid and *cis*-oleic acid were utilized to prepare the stable cobalt oxide nanomaterials. Then, efficiency of these two samples were investigated as a photocatalytic agent in the photodegradation of typical organic pollutant (MG dye) in aqueous solutions. As these are prepared by simple and cheap chemical route i. e. sol-gel process at low temperature which gives good crystallinity and better removal efficiency for the degradation of MG dye [30,31]. Therefore, it may be an alternative for the removal MG dyes from wastewater. In the last section, probable mechanism of photocatalytic activity relied on experimental data have also been anticipated.

## 2. Experimental

### 2.1. 1Materials

Cobalt nitrate (≥98%), citric acid (≥99.5%), oleic acid (≥99%), NaOH (≥99%) and Malachite green (≥90%)were procured from Sigma Aldrich, India. Deionized water was used as a medium. MG (colour Index No. 93405), an anionic dye ($C_{52}H_{54}N_4O_{12}$) was used as model pollutant.

### 2.2. Synthesis of citric acid capped cobalt oxide (CoCA), oleic acid capped cobalt oxide (CoOA) and uncapped cobalt oxide nanoparticles (Co NPs)

In the synthesis of CoCA, CoOA and Co NPs, sol-gel method was used according to reported in previous work [32,33]. A 0.2 M aqueous cobalt nitrate solution was taken as precursor and properly mixed with NaOH till pH = 10 was achieved. Solution of capping agents citric acid and oleic acid were prepared and then stoichiometrically added in already prepared basic solution under constant stirring. After that, the reaction mixture was heated at 75–80 °C for ~16 h till a gel like consistency formed. Then gel was aged for 12 h, and calcined at 190–200 °C in dry air oven for 2–3 h to obtain the nanomaterials of modified cobalt oxide. CoNPs was synthesized without use of any capping agent by using the same procedure.

### 2.3. Photocatalytic activity

Reaction was started at optimum condition. 50 mg of nanocatalysts samples were put in 100 mL of $1 \times 10^{-5}$ M aqueous MG dye under simulated sunlight using xenon lamp with constant light intensity 80 mW/cm$^2$. To prevent thermal radiations circulating water use as coolant. 5 mL of aliquot sample was withdrawn from the mixture at regular intervals, centrifuge and supernatant used for measurement of photocatalytic activity. It was done through UV–visible spectrophotometer by measuring of absorbance of irradiated solution at range of wavelength. % degradation and rate constant were calculated at $\lambda_{max}$ = 610 nm value. Blank experiment with dye also performed to measure photolysis.

### 2.4. Characterization

The powder X-ray diffractometer (PXRD, Bruker AXS D8 Advance) patterns of the Co NPs samples were recorded by using: Cu $K_\alpha$ radiations (wavelength 1.5406 nm) at a 2θ scan rate of 1° per min to indentify the structral phase and crystallite size. The morphology of nanomaterials was evaluated by Scanning electron microscopy (SEM, Model Zeiss EVO 18) and Transmission electron microscopy (TEM, Jeol/JEM 2100, 200 kV power). The absorption spectra were recorded by UV–Vis–NIR spectrophotometer (Cary 5000 Series). The chelating power of the capping agent over the nanomaterial surface were determined from the Fourier transform infrared (FT-IR, Thermo Nicolet, Avatar 370) spectroscopy in ranging of 4000 cm$^{-1}$ to 400 cm$^{-1}$ using KBr pellets and the absorption frequencies were concurrent with the functional groups.

## 3. Results and DISCUSSION

### 3.1. Powder X-ray power differaction (PXRD)

Fig. 1 represents PXRD pattern of synthesized samples which show a series of characteristic peaks situated at 2θ: 20.06 (111), 31.4 (220), 37.04 (311), 45.06 (400), 59.3 (511), 65.38 (440) of all samples of synthesized cobalt oxide. These planes match well with the FCC phase and Fd3m space group (spinel like $Fe_3O_4$) with JCPDS file no. 01-078-1970. Among them, few small impurity peaks were observed due to presence of citrate/oleate etc. $Co_3O_4$ spectra show sharp peaks with higher degree of crystallinity. The crystalline size (D)was evaluated by using the Debye–Scherrer expression as given below:

$$D = \frac{K\lambda}{\beta\, Cos\theta} \quad (1)$$

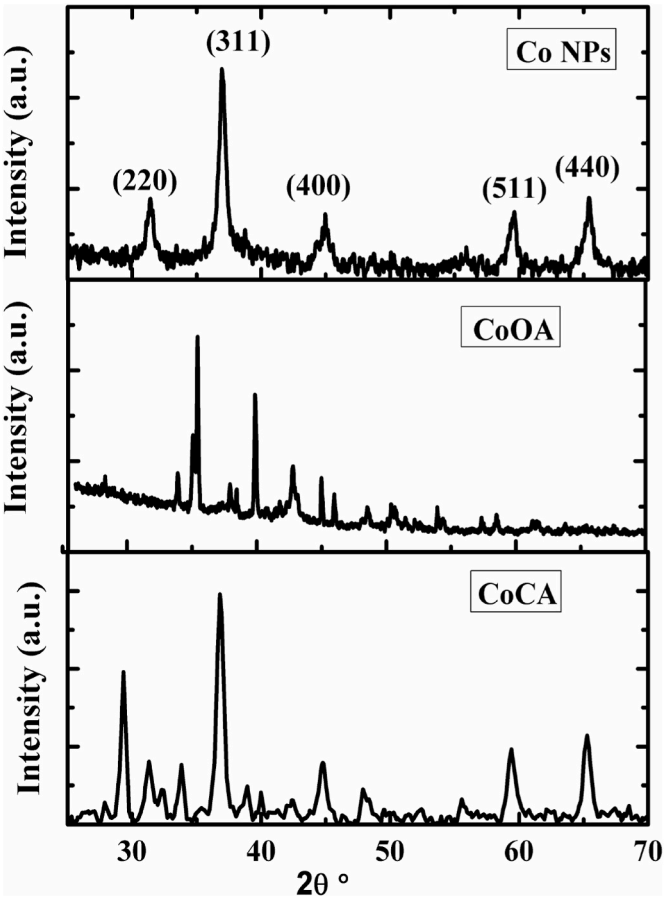


**Fig. 1.** PXRD of CoCA, CoOA and CoNPs.

where, K is equal to 0.94 indicating Scherrer constant, λ is the used X-ray wavelength and equal to 1.540 Å, β is full width at half-maximum (FWHM), and θ is the angle of Bragg diffraction (Degree). The measured D was 29 and 42 nm for CoCA, CoOA respectively.

### 3.2. Scanning electron microscopy (SEM)

Citric acid is a good chelating agent having four denticity sites that facilitated spherical shapes of particles by surface functionalization. Fig. 2a shows the SEM micrographs of CoCA powder having morphology as constituting of layered porous aggregates and superimposed. Their porous structures exposed greater surface area. Oleic acid is another a good agent using in capping that binded powerfully with the surface of the metal through the $COO^{-}$ and played a important role in the growth and stability of particles and inhibit further oxidation. Fig. 2b shows the flake like aggregates morphology of CoOA. They are also porous and constituted nanosheets. Co NPs powder (Fig. 2c) has no specific morphology and show high agglomeration.

### 3.3. Transmission electron microscopy (TEM)

TEM of CoCA represent continuous morphology with the average particle size was 30 nm. SAED pattern of CoCA has been given in Fig. 3, where the distinct diffraction rings with bright sharp spots correspond to the high degree of crystallinity than that of the other samples. In CoOA image the particles were discrete and polydisperse with size ranging from 8 to 12 nm. The TEM sizes were in close agreement with average crystallite ($D_{XRD}$), indicating that the synthesized nanoparticles did not coalesce into larger crystallites after calcination.

### 3.4. UV-spectroscopy

Fig. 4 shows the absorption spectra for the capped and uncapped samples. The absorption curves for the samples showed two strong bands at 250–350 and 400–580 nm. The first band occurs due to charge transfer process between $O^{2-}$ to $Co^{2+}$ while other one corresponds $O^{2-}$ to $Co^{3+}$ [34]. Absorption spectra, peaks were without any prominent blue shift due to uneven distribution of the particles. However, the CoCA showed higher and CoOA represented lower absorption than CoP. This can be explained by different morphology and size of particles by capping agents [35].

### 3.5. FT-IR spectroscopy

As compare with pure citric acid [36] and oleic acid [37] spectra, absorption bands of capped samples are highly resolved as shown in Fig. 5. Due to chelation of capping agent with Co NPs nanomaterials, CoCA and CoOA showed broader and low transmittance peaks. The broad absorption band centred around 3400 $cm^{-1}$ was due to –OH stretching vibrations of absorbed moisture available in all samples. Two bands around 1650 and 1558 $cm^{-1}$ exhibited of the symmetric and asymmetric $–COO^{-}$ vibrations [37]. These group also involved in esterification reaction with hydroxyl groups present on the Co NPs surface [38], that gave partial double bond feature to –C═O group. –C═C–stretching peak of oleic acid was disappeared due to merging with carbonyl group [34]. Sharp shoulders at 2925 and 2852 $cm^{-1}$ found in CoOA spectrum only, that corresponded symmetric and asymmetric stretching vibrations of $–CH_2$ of oleic acid. These peaks were although present but very weak in the CoCA spectrum due to less alkyl groups. The sharp intense absorption band situated at 1383 $cm^{-1}$ might possibly be ascribed to the bending vibrations of $–CH_2$ groups in both spectra. Also, the sharp peak at 880 $cm^{-1}$ could be due to out of plane bending vibration of –CH and –OH. The sharp bands around 573 and 662 $cm^{-1}$ characteristic of Co–O stretching vibration and O–Co–O bridging vibration respectively as observed in the all spectra [39].

### 3.6. Thermogravimetric analysis (TGA)

CoCA samples showed weight loss up to 13% while CoOA showed less than 10% weight loss till 200 °C as shown in Fig. 6. This decrement corresponding to the elimination of moisture and desorption of physi-osorbed water. Samples exhibited a broad plateau, around 200 °C, indicating thermal stability of the samples, in this temperature range. Hence, it could be concluded that the surface coated capping ligands of the samples were intact and did not decompose till 200 °C. Above 200 °C decomposition of the capping functional groups began.

### 3.7. Photocatalytic activity

The decrement in the absorbance values of the MG dye could be related with the photodegradation. The degradation efficiency was calculated by following expression and represented in Fig. 8.

$$\%\ Degradation = 100 \times \frac{(Ao - A)}{Ao} \quad (2)$$

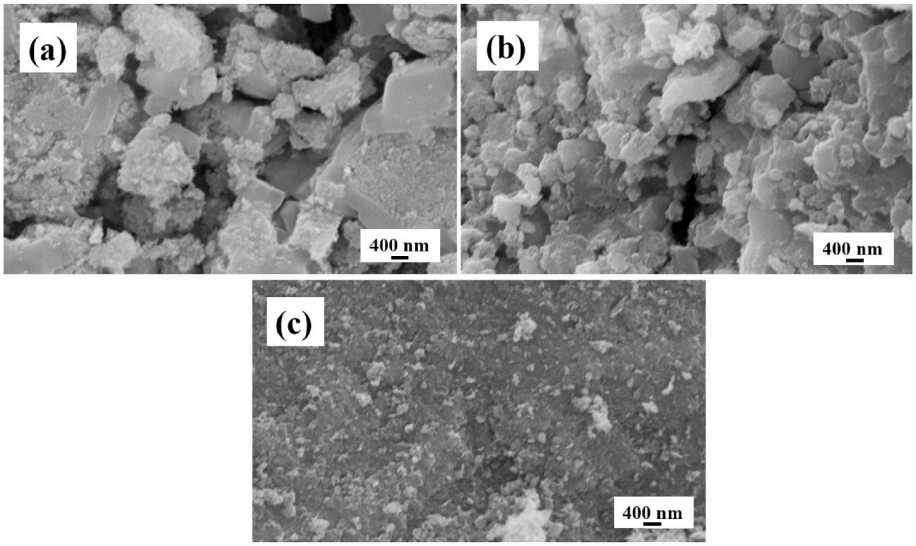


**Fig. 2.** SEM micrographs of Samples (a) CoCA (b) CoOA (c) Co NPs.

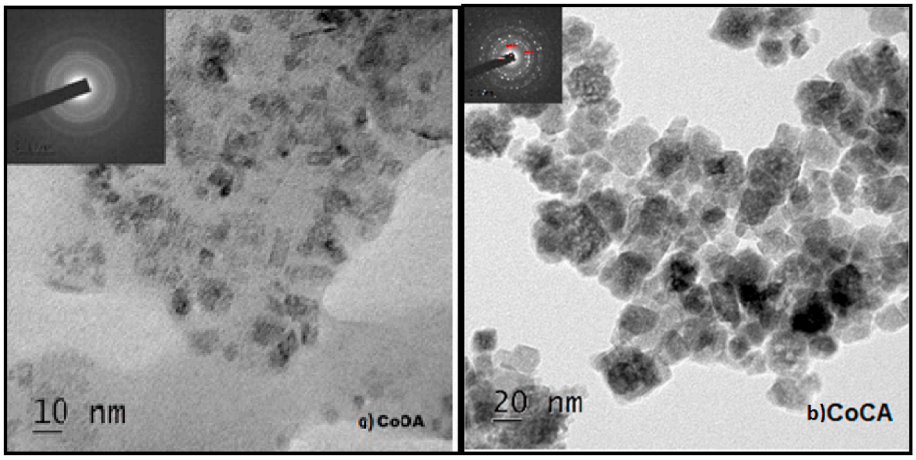


**Fig. 3.** TEM image of CoCA and CoOA.

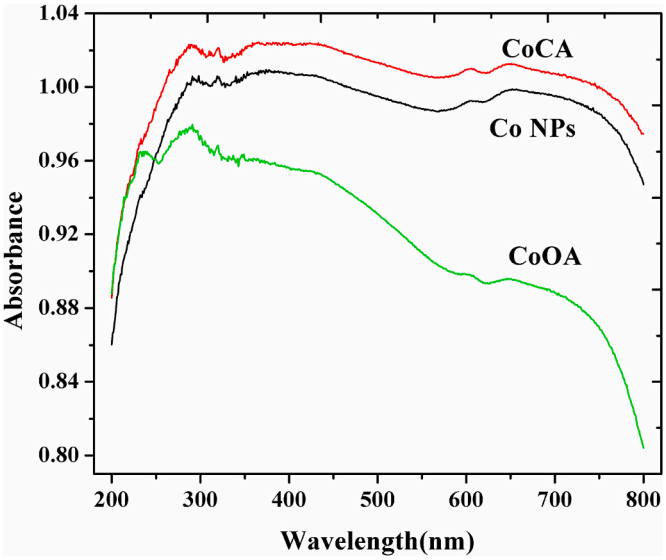


**Fig. 4.** Absorption spectra of CoCA, CoOA and CoNPs.

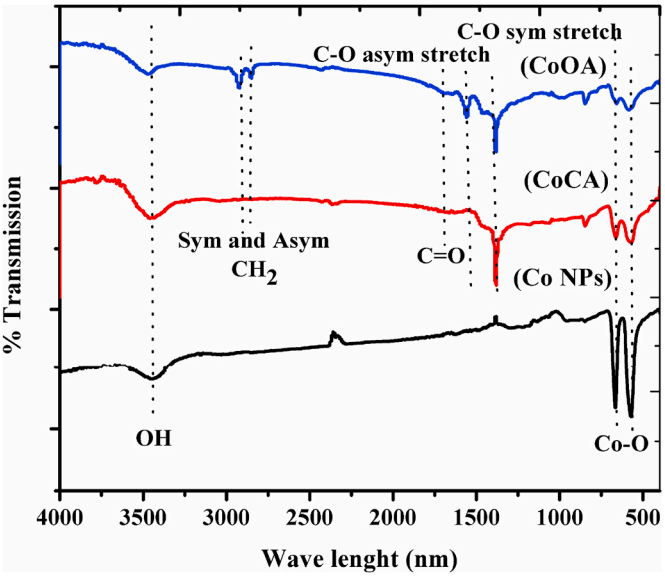


**Fig. 5.** FTIR spectrum of CoCA, CoOA and CoNPs.

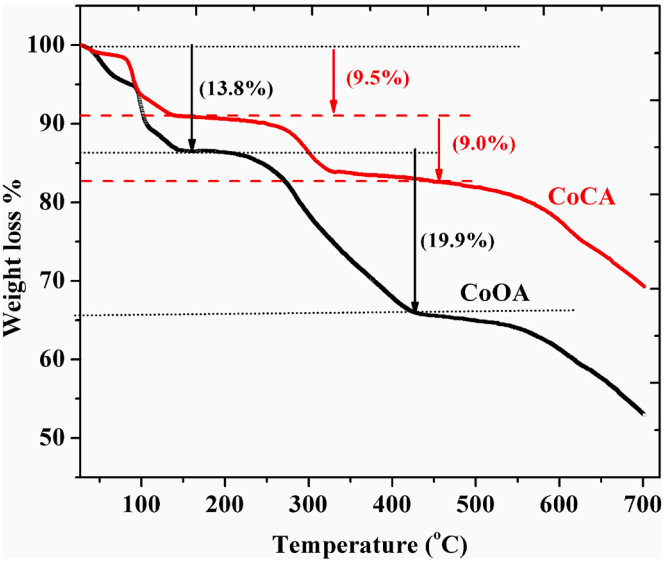


**Fig. 6.** TGA analysis of CoCA and CoOA samples.

where, $A_O$ and A are the dye absorbance before and after of photocatalytic reaction.

Fig. 7 (a) and (b) display the time dependent photocatalytic degradation of MG dye for the samples under visible light irradiation. The curves represent the linear fitting of pseudo-first-order [40] and pseudo-second-order reaction [41] kinetics which is represented by following expressions:

$$k_1 = \frac{1}{t}\ln(A / Ao) \quad (3)$$

$$k_2 = \frac{1}{t}\left[\frac{1}{A} - \frac{1}{Ao}\right] \quad (4)$$

The kinetics results are shown in Table 1. From the results, the value of $R^2$ is closed to pseudo-second-order kinetics in the MG dye degradation. The CoCA photocatalyst was found to be more efficient for dye degradation compared to the CoOA. The overall order of efficiency of photocatalytic activity for the samples was as follow: CoCA > CoOA > Co NPs as display in Table 1. After 100 min of irradiation, the photocatalytic degradation activity shown by CoCA was 24.6% greater than that of CoOA, which could be associated with higher stability, increased surface area and more dispersion per unit volume in aqueous solution due to less hydrophobic character of the surface of citric acid than the

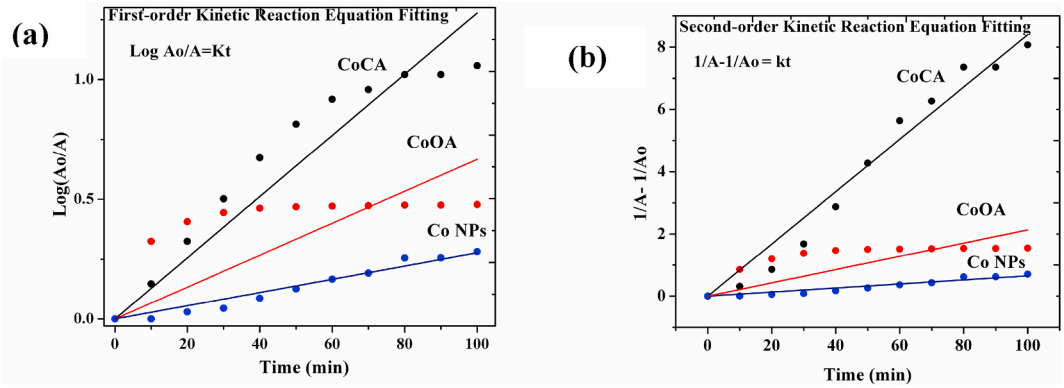


**Fig. 7.** The fitting curves of the (a) pseudo-first order, and (b) pseudo-second-order kinetics model for MG dye with CoCA, CoOA and Co NPs.

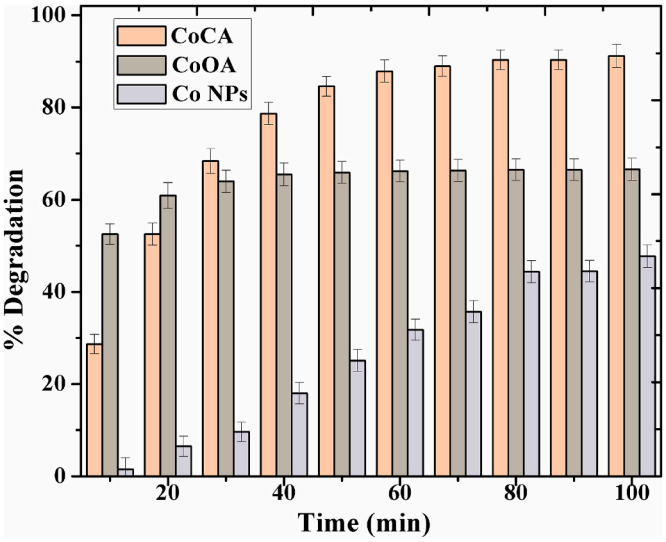


**Fig. 8.** Effect of time on photocatalytic degradation of MG dye with CoCA, CoOA and CoNPs.

**Table 1**
The value of rate constants and % degradation of MG Dye by solar/nano Co NPs.

| Samples | First-order kinetic fitting | | Second-order kinetic fitting | | % Degradation |
|---|---|---|---|---|---|
| | k ($min^{-1}$) | $R^2$ | k ($mol^{-1}L^1min^{-1}$) | $R^2$ | |
| CoCA | 0.01278 | 0.9714 | 0.00653 | 0.9882 | 91.2 |
| CoOA | 0.00666 | 0.8280 | 0.084 | 0.8533 | 66.6 |
| CoNPs | 0.00277 | 0.9620 | 0.00653 | 0.9671 | 47.7 |

case for oleic acid.

Amphiphilic molecule like oleic acid got chemisorbed as carboxylate onto nanoparticles surface and surround it by vertical attachment forming surface monolayers and hence the surface properties of Co NPs change from hydrophilic to hydrophobic which stabilized them against agglomeration and aggregation and this also prevented from air oxidation [37].

Citric acid molecule through four donor sites can easily coordinate metallic ions to form chelating ring. This would encourage the formation of several types of titanium complexes [42].

Porous structures favor photocatalysis by increasing the surface area that facilitate the dye molecule to penetrate the surface of catalyst and promote short diffusion path length of photogenerated charge carriers that lead to higher photocatalytic activity [25]. Hence, nanosized CoCA catalyst produced good performance in the photocatalytic degradation of MG dye.

## 4Probable mechanism

From the experimental results and reported literature reveal [33], a tentative mechanism for the photocatalytic degradation of MG dye by modified $Co_3O_4$ nanomaterials was examined. The reaction sequences are given below:

$$MG^{*}_{ads} + Co_3O_4 \rightarrow MG^{\cdot+} + Co_3O_4(e^-) \quad (5)$$

$$Co_3O_4(e^-) + O_2 \rightarrow O_2^{\cdot-} \quad (6)$$

$$Co_3O_4(h^-) + OH^- \rightarrow OH^{\cdot} \quad (7)$$

$$OH^{\cdot} \text{ or } O_2^{\cdot-} + MG^{\cdot+} \rightarrow degradation\ products \quad (8)$$

$$OH^{\cdot} \text{ or } O_2^{\cdot-} + MG^{*}_{ads} \rightarrow degradation\ products \quad (9)$$

With the absorption of light MG dye excited and shifted electrons to the conduction band of Co NPs. These electrons are scavenged by dissolved oxygen to produce highly reactive superoxide oxygen radical anion ($O_2^{\bullet-}$). These $O_2^{\bullet-}$ can react with the adsorbed moisture of the surface to produce $H_2O_2$ which is finally converted into $^{\bullet}OH$. Hence, $O_2^{\bullet-}$ and $^{\bullet}OH$ radicals might be responsible for dye degradation. In this case, $^{\bullet}OH$ did not participate in reaction since the degradation rate of MG did not reduce by the existence of $^{\bullet}OH$ scavenger (2−propanol). Hence, $O_2^{\bullet-}$ was the main oxidizing moieties which causes oxidation of compounds and leads to mineralization.

## 5. Conclusions

Role of citric acid and oleic acid as capping agents was ceased the particles growth rate by forming surface complexes and stabilized nanomaterials, and, then photocatalytic degradation of MG dye by modified Co NPs was investigated. The results revealed that citric acid capped cobalt oxide exhibited higher photocatalytic activity for the photodegradation of MG dye. The pollutant MG undergoes 91.2% and 66.6% degradation in presence of CoCA and CoOA, respectively while it was only 47.7% with $Co_3O_4$ nanoparticles. CoOA exhibited lower activity due to its morphology having lack stacked nanolayer structure which exposes lesser surface area as compared to nanograin structure of CoCA. The value of MG dye degradation rate was higher for both samples against pure one. The introduction of larger number of chelating sites in the capping molecules also provided superior stability to nanomaterials and a synergistic effect on their photocatalytic ability. Therefore, synthesized materials can be used for the photocatalytic degradations of other cationic and anionic dyes such as Rodhamine B

(RB), Congo Red (CR), Methylene blue (MB), Methyl Orange (MO) etc.

## CRediT authorship contribution statement

**Monu Verma:** Formal analysis, editing draft. **Meena Mitan:** Investigation, Data curation, Formal analysis, Writing – original draft. **Hyunook Kim:** Supervision, Validation, Visualization. **Dipti Vaya:** Conceptualization, Supervision, Validation, Visualization, editing draft.

## Declaration of competing interest

The authors declare that they have no known competing financialinterestsor personal relationships that could have appeared to influence the work reported in this paper.

## Acknowledgements

Authors thank STIC, Kerala for providing FT-IR and XRD facility and IIT Delhi for SEM facility. Dipti Vaya acknowledges the support provided under the DST-FIST Grant No. SR/FST/PS-I/2019/68 of Govt. Of India. Monu Verma thankful to National Research Foundation of Korea (NRF) for providing funding by the Ministry of Science and ICT under the Brain Pool Program (2019H1D3A1A01102657).

## References

[1] M. Verma, K.P. Singh, A. Kumar, Reactive magnetron sputtering based synthesis of WO3 nanoparticles and their use for the photocatalytic degradation of dyes, Solid State Sci. 99 (2020) 105847, https://doi.org/10.1016/j.solidstatesciences.2019.02.008.

[2] M. Iqbal, Vicia faba bioassay for environmental toxicity monitoring: a review, Chemosphere 144 (2016) 785–802, https://doi.org/10.1016/j.chemosphere.2015.09.048.

[3] M. Abbas, M. Adil, S. Ehtisham-ul-Haque, B. Munir, M. Yameen, A. Ghaffar, G. A. Shar, M. Asif Tahir, M. Iqbal, Vibrio fischeri bioluminescence inhibition assay for ecotoxicity assessment: a review, Sci. Total Environ. 626 (2018) 1295–1309, https://doi.org/10.1016/j.scitotenv.2018.01.066.

[4] M. Iqbal, M. Abbas, J. Nisar, A. Nazir, Bioassays based on higher plants as excellent dosimeters for ecotoxicity monitoring: a review, Chem. Int. 5 (2019) 1–80.

[5] O.J. Hao, H. Kim, P.C. Chiang, Decolorization of wastewater, Crit. Rev. Environ. Sci. Technol. 30 (2000) 449–505, https://doi.org/10.1080/10643380091184237.

[6] G. Pilaniya, P. Rawat, D. Vaya, Chapter 1Malachite green :recent development. Malachite Green Prop. Uses, 2020, pp. 1–38.

[7] S. Srivastava, R. Sinha, D. Roy, Toxicological effects of malachite green, Aquat. Toxicol. 66 (2004) 319–329, https://doi.org/10.1016/j.aquatox.2003.09.008.

[8] W. Cheng, S. Wang, L. Lu, W. Gong, X. Liu, B. Gao, H. Zhang, Removal of malachite green ( MG ) from aqueous solutions by native and heat-treated anaerobic granular sludge, Biochem. Eng. J. 39 (2008) 538–546, https://doi.org/10.1016/j.bej.2007.10.016.

[9] A. Ayach, S. Fakhi, Z. Faiz, A. Bouih, O.A. Malek, A. Benkdad, M. Benmansour, A. Laissaoui, M. Adjour, Y. Elbatal, I. Vioque, G. Manjon, Adsorption of methylene blue on bituminous schists from Tarfaya-Boujdour, Chem. Int. 3 (2019) 442–451, https://doi.org/10.31221/osf.io/n29sq.

[10] K.B. Daij, S. Bellebia, Z. Bengharez, Comparative experimental study on the COD removal in aqueous solution of pesticides by the electrocoagulation process using monopolar iron electrodes, Chem. Int. (2019) 420–427, https://doi.org/10.31221/osf.io/zcas9.

[11] K. Djehaf, A.Z. Bouyakoub, R. Ouhib, H. Benmansour, A. Bentouaf, A. Mahdad, N. Moulay, D. Bensaid, M. Ameri, Textile wastewater in Tlemcen (Western Algeria): impact, treatment by combined process, Chem. Int. 3 (2019) 414–419, https://doi.org/10.31221/osf.io/q3jvy.

[12] F. Minas, B.S. Chandravanshi, S. Leta, Chemical precipitation method for chromium removal and its recovery from tannery wastewater in Ethiopia, Chem. Int. 3 (2019) 392–405, https://doi.org/10.31221/osf.io/m7h5k.

[13] A. Chham, E. Khouya, M. Oumam, A. Abourriche, S. Gmouh, S. Mansouri, N. Elhammoudi, N. Hanafi, H. Hannache, The use of insoluble matter of Moroccan oil shale for removal of dyes from aqueous solution, Chem. Int. 4 (2019) 67–76, https://doi.org/10.31221/osf.io/x4v9p.

[14] A.G.S. Prado, L.L. Costa, Photocatalytic decouloration of malachite green dye by application of TiO2 nanotubes, J. Hazard Mater. 169 (2009) 297–301, https://doi.org/10.1016/j.jhazmat.2009.03.076.

[15] S. Gora, Y.N. Zhou, A. Sokolowski, M. Hatat-fraile, R. Liang, Solar photocatalysis with modified TiO2 photocatalysts : effects on NOM and disinfection byproduct formation potential, Environ. Sci. Water Res. Technol. 4 (2018) 1361–1376, https://doi.org/10.1039/c8ew00161h.

[16] K.S. Babu, A.R. Reddy, K.V. Reddy, Controlling the size and optical properties of ZnO nanoparticles by capping with SiO2, Mater. Res. Bull. 49 (2014) 537–543, https://doi.org/10.1016/j.materresbull.2013.09.024.

[17] P. Gupta, N.K. Pandey, K. Kumar, B. Yadav, Structural, optical and LPG sensing properties of zinc-doped nickel oxide pellets operated at room temperature, Sensors Actuators A Phys 319 (2021) 112484.

[18] U. Kamran, H.N. Bhatti, M. Iqbal, A. Nazir, Green synthesis of metal nanoparticles and their applications in different fields: a review, Zeitschrift Fur Phys. Chemie. 233 (2019) 1325–1349, https://doi.org/10.1515/zpch-2018-1238.

[19] S.L. Gaikwad, A.P. Angre, V.A. Naik, J.G. Pargaonkar, P.A. Patil, K.V. Chandekar, A.U. Chavan, P.S. Gaikar, Binderless synthesis of nanoknotnet-like cobalt oxide for supercapacitor application, Mater. Today Proc (2020), https://doi.org/10.1016/j.matpr.2020.04.081.

[20] C.S. Jincy, P. Meena, Synthesis, characterization, and NH3 gas sensing application of Zn doped cobalt oxide nanoparticles, Inorg. Chem. Commun. 120 (2020) 108145, https://doi.org/10.1016/j.inoche.2020.108145.

[21] J. Huang, H. Ren, K. Chen, J.J. Shim, Controlled synthesis of porous Co3O4 micro/nanostructures and their photocatalysis property, Superlattice. Microst. 75 (2014) 843–856, https://doi.org/10.1016/j.spmi.2014.09.006.

[22] K.V.K. Rao, Inhibition of DNA synthesis in primary rat hepatocyte cultures by malachite green: a new liver tumor promoter, Toxicol. Lett. 81 (1995) 107–113, https://doi.org/10.1016/0378-4274(95)03413-7.

[23] N. Akhlaghi, G. Najafpour-Darzi, H. Younesi, Facile and green synthesis of cobalt oxide nanoparticles using ethanolic extract of Trigonella foenumgraceum (Fenugreek) leaves, Adv. Powder Technol. 31 (2020) 3562–3569, https://doi.org/10.1016/j.apt.2020.07.004.

[24] I. Bibi, N. Nazar, M. Iqbal, S. Kamal, H. Nawaz, S. Nouren, Y. Safa, K. Jilani, M. Sultan, S. Ata, F. Rehman, M. Abbas, Green and eco-friendly synthesis of cobalt-oxide nanoparticle: characterization and photo-catalytic activity, Adv. Powder Technol. 28 (2017) 2035–2043, https://doi.org/10.1016/j.apt.2017.05.008.

[25] R. Edla, N. Patela, M. Orlandi, N. Bazzanella, V. Bello, C. Maurizio, G. Mattei, P. Mazzoldi, A. Miotello, Highly photo-catalytically active hierarchical 3D porous/urchin nanostructured Co3O4 coating synthesized by Pulsed Laser Deposition, Appl. Catal. B Environ. 166–167 (2015) 475–484, https://doi.org/10.1016/j.apcatb.2014.11.060.

[26] W. Wen, J.M. Wu, J.P. Tu, A novel solution combustion synthesis of cobalt oxide nanoparticles as negative-electrode materials for lithium ion batteries, J. Alloys Compd. 513 (2012) 592–596, https://doi.org/10.1016/j.jallcom.2011.11.019.

[27] M. Parashar, V.K. Shukla, R. Singh, Metal oxides nanoparticles via sol–gel method: a review on synthesis, characterization and applications, J. Mater. Sci. Mater. Electron. 31 (2020) 3729–3749, https://doi.org/10.1007/s10854-020-02994-8.

[28] E.G. Goh, X. Xu, P.G. McCormick, Effect of particle size on the UV absorbance of zinc oxide nanoparticles, Scripta Mater. (2014) 78–79, https://doi.org/10.1016/j.scriptamat.2014.01.033, 49–52.

[29] P. Chandrasekaran, G. Viruthagiri, N. Srinivasan, The effect of various capping agents on the surface modifications of sol-gel synthesised ZnO nanoparticles, J. Alloys Compd. 540 (2012) 89–93, https://doi.org/10.1016/j.jallcom.2012.06.032.

[30] M. Amiri, M. Salavati-Niasari, A. Akbari, T. Gholami, Removal of malachite green (a toxic dye) from water by cobalt ferrite silica magnetic nanocomposite: herbal and green sol-gel autocombustion synthesis, Int. J. Hydrogen Energy 42 (2017) 24846–24860, https://doi.org/10.1016/j.ijhydene.2017.08.077.

[31] A.S. Hassanien, A.A. Akl, A.H. Sáaedi, Synthesis, crystallography, microstructure, crystal defects, and morphology of BixZn1-xO nanoparticles prepared by sol-gel technique, CrystEngComm 20 (2018) 1716–1730, https://doi.org/10.1039/c7ce02173a.

[32] M. Pudukudy, Z. Yaakob, Sol-gel synthesis, characterisation, and photocatalytic activity of porous spinel Co3O4 nanosheets, Chem. Pap. 68 (2014) 1087–1096, https://doi.org/10.2478/s11696-014-0561-7.

[33] S. Meena, D. Vaya, B.K. Das, Photocatalytic degradation of Malachite Green dye by modified ZnO nanomaterial, Bull. Mater. Sci. 39 (2016) 1735–1743, https://doi.org/10.1007/s12034-016-1318-4.

[34] T. He, D. Chen, X. Jiao, Y. Wang, Y. Duan, Solubility-controlled synthesis of high-quality Co3O4 nanocrystals, Chem. Mater. 17 (2005) 4023–4030, https://doi.org/10.1021/cm050727s.

[35] C.V. Restrepo, V.C. Cristian, Synthesis of silver nanoparticles, influence of capping agents, and dependence on size and shape: a review, Environ. Nanotechnology, Monit. Manag. (2021) 100428, https://doi.org/10.1016/J.ENMM.2021.100428.

[36] E. Cheraghipour, S. Javadpour, A.R. Mehdizadeh, Citrate capped superparamagnetic iron oxide nanoparticles used for hyperthermia therapy, J. Biomed. Sci. Eng. 5 (2012) 715–719.

[37] R. Ramos-gonzález, L.A. García-cerda, M.A. Quevedo-lópez, Study of the surface modification with oleic acid of nanosized HfO2 synthesized by the polymerized complex derived sol – gel method, Appl. Surf. Sci. 258 (2012) 6034–6039, https://doi.org/10.1016/j.apsusc.2012.02.122.

[38] L. Sun, H. Li, L. Ren, C. Hu, Synthesis of Co3O4 nanostructures using a solvothermal approach, Solid State Sci. 11 (2009) 108–112, https://doi.org/10.1016/j.solidstatesciences.2008.05.013.

[39] J.C. Liu, J.H. Jean, C.C. Li, Dispersion of nano-sized γ-alumina powder in non-polar solvents, J. Am. Ceram. Soc. 89 (2006) 882–887, https://doi.org/10.1111/j.1551-2916.2005.00858.x.

[40] D. Vaya, Meena, B.K. Das, Green synthesis of cobalt oxide nanoparticles by a starch-assisted method, nanosci, Nanotechnology-Asia 9 (2019) 362–370.
[41] M. Verma, A. Kumar, C. Singh, Krishna Pal Srivastava, V. Rawat, S. Rao, Gyandeshwar Kumari, P. Sharma, H.S. Kim, Graphene oxide-manganese ferrite (GO-MnFe2O4) nanocomposite: one-pot hydrothermal synthesis and its use for adsorptive removal of Pb2+ ions from aqueous medium, J. Mol. Liq. 315 (2020) 113769.
[42] W. Li, J. Li, X. Wang, J. Ma, Q. Chen, Effect of citric acid on photoelectrochemical properties of tungsten trioxide films prepared by the polymeric precursor method, Appl. Surf. Sci. 256 (2010) 7077–7082, https://doi.org/10.1016/j.apsusc.2010.05.030.